

# Oersted-field-induced switching of a ferromagnet on a Si substrate via localized dielectric breakdown of the native SiO<sub>2</sub> layer

N. I. Polushkin, M. V. Sapozhnikov, N. S. Gusev, S. N. Vdovichev, and M. N. Drozdov

Citation: *Appl. Phys. Lett.* **111**, 012401 (2017); doi: 10.1063/1.4990975

View online: <http://dx.doi.org/10.1063/1.4990975>

View Table of Contents: <http://aip.scitation.org/toc/apl/111/1>

Published by the [American Institute of Physics](#)

---

---



**THE WORLD'S RESOURCE FOR  
VARIABLE TEMPERATURE  
SOLID STATE CHARACTERIZATION**



OPTICAL STUDIES SYSTEMS



SEEBECK STUDIES SYSTEMS



MICROPROBE STATIONS



HALL EFFECT STUDY SYSTEMS AND MAGNETS



[WWW.MMR-TECH.COM](http://WWW.MMR-TECH.COM)

# Oersted-field-induced switching of a ferromagnet on a Si substrate via localized dielectric breakdown of the native SiO<sub>2</sub> layer

N. I. Polushkin, M. V. Sapozhnikov, N. S. Gusev, S. N. Vdovichev, and M. N. Drozdov

*Institute for Physics of Microstructures of Russian Academy of Sciences, 603950 GSP-105, Nizhny Novgorod, Russia*

(Received 1 March 2017; accepted 18 June 2017; published online 5 July 2017)

The phenomenon of dielectric breakdown is employed for switching of magnetization in ferromagnetic (FM) metallic layers of Co and CoFe sputtered onto the native oxide (SiO<sub>2</sub>) of Si substrates of different types. The switching can occur even without applying a bias field under discharging a capacitor through an FM/SiO<sub>2</sub>/Si sample via electric pads lying on its surface. The switching thresholds and biasing fields (if needed) are found to be much lower in samples based on low-resistivity ( $\sim 10$  m $\Omega$  cm) substrates. It is argued that the discharge induces localized breakdown of the SiO<sub>2</sub> layer, and so, the discharge current is able to flow through the Si substrate. This current produces the magnetic (Oersted) field inside the FM layer, which is sufficient for the switching. Such on-chip pulsed magnetic fields generated in FM/SiO<sub>2</sub>/Si structures can be employed instead of bulky electromagnets for developing magnetic technologies, which would be compatible with Si-based electronics. *Published by AIP Publishing.* [<http://dx.doi.org/10.1063/1.4990975>]

A reason for successful integration of Si-based devices into the field of microelectronics is the occurrence of a Si dioxide (SiO<sub>2</sub>) layer on the surface of a Si wafer, which serves as an insulator and as a protecting passivation layer.<sup>1</sup> It is also of considerable interest<sup>2</sup> that this ability of SiO<sub>2</sub> adds functionalities to metal-oxide-semiconductor (MOS) structures by combining it with the phenomenon of dielectric breakdown<sup>3–5</sup> observed by applying a strong enough electric field ( $>10^5$  kV/m). A manifestation of dielectric breakdown is the irreversible immense decrease in electrical resistance of the system owing to the formation of percolation paths in which the chemical structure of SiO<sub>2</sub> is modified.<sup>6–8</sup> In MOS devices, this effect has been studied for decades in the context of reliability and device failure<sup>5</sup> and more recently<sup>9</sup> has been investigated for applications in non-volatile memory. Here, we demonstrate that breakdown in MOS structures can be used for the generation of a magnetic (Oersted) field which is able to switch magnetization in the ferromagnetic (FM) layer, that is, metallic component of the MOS structure (FM/SiO<sub>2</sub>/Si). We explore how discharging a capacitor through the FM/SiO<sub>2</sub>/Si structure affects its magnetization.<sup>10</sup> We show that magnetization switching induced by the discharge results from the breakdown of the SiO<sub>2</sub> layer on the Si surface. The discharge current starts to flow through the Si substrate and generates the Oersted field  $\mathbf{B}_{OE}$  that toggles magnetization in the FM layer sputtered onto SiO<sub>2</sub>/Si. Electrical control of magnetism has emerged as an appealing solution to significantly reduce the power dissipation and variability beyond current MOS technology.<sup>11–14</sup> It is here challenging to get a candidate with high Curie temperature, controllable ferromagnetism, and easy integration with current Si-based electronics.

The samples studied here are FM metallic layers of CoFe and Co sputtered in a vacuum chamber<sup>15</sup> onto natively oxidized 400- $\mu$ m-thick Si substrates. These two FM materials are chosen as being extensively used for controlling the magnetism with electrical means.<sup>12,14,16</sup> The obtained results

are demonstrated with two different samples, a 15-nm-thick CoFe film on a Si substrate of *n* type (Si-*n*) with a resistivity of  $\rho_{Si} = 5.0$  m $\Omega$  cm and a 20-nm-thick Co film on a Si wafer of *p* type (Si-*p*) with a resistivity of  $\rho_{Si} = 12$  m $\Omega$  cm. For comparison, CoFe and Co layers with the same thicknesses, i.e., 15 and 20 nm, respectively, were prepared on high-resistivity ( $\rho_{Si} = 10$   $\Omega$  cm) Si-*p* substrates under the same other sputtering conditions.

To control the native oxide on the Si surface, we analyzed the chemical composition of our samples in their depth using secondary ion mass spectroscopy (SIMS). The SIMS procedures performed are described in Ref. 17. Also, the formation of the native SiO<sub>2</sub> layer on the Si surface was detected for the electrical resistance of both reference samples, i.e., SiO<sub>2</sub>/Si and FM/SiO<sub>2</sub>/Si. The magnetic properties of FM films sputtered onto SiO<sub>2</sub>/Si were controlled with the longitudinal magneto-optic Kerr effect (MOKE). The schematic of the experimental geometry is shown in Fig. 1. Two Al pads with a width of  $W \sim 1.0$  mm (black boxes) were

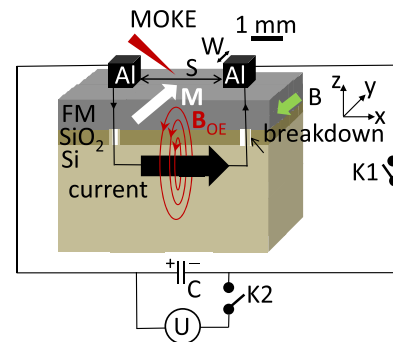


FIG. 1. Schematic of the experiments on magnetization switching in FM/SiO<sub>2</sub>/Si samples via the localized breakdown of the SiO<sub>2</sub> layer under discharging the capacitor *C*. The discharge current starts to flow along the *x* axis in the Si substrate and produces the Oersted field  $\mathbf{B}_{OE}$  that toggles magnetization  $\mathbf{M}$  oriented in the film plane along the *y* axis, if  $\mathbf{B}_{OE}$  (and assisting  $\mathbf{B}$  when needed) is aligned antiparallel to the initial direction of  $\mathbf{M}$ .

placed on the sample surface at pad-to-pad spacings ( $S$ ) varying in a range of 1.0 to 5.0 mm. The magnetization in the interpad gap was probed *in situ* with MOKE both before and after discharging a capacitor ( $C$ ) through the sample upon closing switch K1.<sup>18</sup> The discharge current flowing in the substrate decays in time as  $(U/2R_{\perp})\exp(-t/2R_{\perp}C)$ , where  $U$  is the voltage applied for charging the capacitor when switches K2 and K1 are closed and opened, respectively, and  $2R_{\perp}$  is the resistance to the discharge.

Figure 2(a) shows the results of SIMS depth profiling of the atomic/molecular distributions of O, Si, SiO, and SiO<sub>2</sub> in a 15-nm-thick CoFe layer sputtered onto a Si- $n$  (111) substrate with a resistivity of  $\rho_{\text{Si}} = 5.0 \text{ m}\Omega \text{ cm}$ . These data indicate that the native oxide remains on the Si surface after sputtering and that SiO<sub>2</sub> gives the major contribution to its composition. We also see that the concentration of oxygen increases at both the surfaces of the CoFe layer. Obviously, the oxygen enhancement at the outer surface can be attributed to the formation of the corrosion (oxide/hydroxide) layer,<sup>10</sup> while its increase at the inner (CoFe/Si- $n$ ) surface reflects the occurrence of the oxide layer between the metal and Si- $n$ . The obtained SIMS data allow us to draw a sketch of the sample structure, as shown in the inset of Fig. 2(a). Interestingly, similar concentration profiles—with practically the same thickness of the SiO<sub>2</sub> layer ( $\sim 5.0 \text{ nm}$ )—were observed in our SIMS studies of the samples sputtered onto Si substrates of other types used, e.g., highly resistive ( $\rho_{\text{Si}} = 10 \Omega \text{ cm}$ ) Si- $p$  (100) (not shown).

To demonstrate the electrical breakdown of the native SiO<sub>2</sub> layer under electrical discharges (Fig. 1), we have measured the two- and four-probe resistances of our samples in their as-prepared state and after discharges at different  $U/S$  values. Figure 2(b) depicts the two-probe resistance, measured between the pads used for magnetization switching

(Fig. 1), of reference samples—SiO<sub>2</sub>/Si- $n$  ( $\rho_{\text{Si}} = 5.0 \text{ m}\Omega \text{ cm}$ ) and SiO<sub>2</sub>/Si- $p$  ( $\rho_{\text{Si}} = 10 \Omega \text{ cm}$ )—and of the same reference samples covered by a CoFe layer (CoFe/SiO<sub>2</sub>/Si). We see that, after discharges of  $C = 5.0 \mu\text{F}$  at  $U/S > 15 \text{ kV/m}$ , the two-probe resistance of the reference sample comprised of the low-resistivity Si- $n$  ( $\rho_{\text{Si}} = 5.0 \text{ m}\Omega \text{ cm}$ ) strongly decreases from its initial value of a few megaohms and asymptotically approaches  $\approx 5.0 \Omega$  at  $U/S > 100 \text{ kV/m}$ . A similar behavior has been found in the CoFe/SiO<sub>2</sub>/Si- $n$  ( $\rho_{\text{Si}} = 5.0 \text{ m}\Omega \text{ cm}$ ) sample where the initial two-probe resistance,  $\sim 30 \Omega$ , decreases down to the same value, i.e.,  $\approx 5.0 \Omega$ . The observed decrease in the two-probe resistance and vanishing of a difference in this quantity between SiO<sub>2</sub>/Si and FM/SiO<sub>2</sub>/Si after discharges can be attributed to the breakdown of SiO<sub>2</sub> in both kinds of samples. Importantly, breakdown occurs locally, i.e., underneath the pads. If we change the pad location for any other one where the SiO<sub>2</sub> layer is virgin, a highly resistive state will be found again. In contrast to a low-resistivity Si and thin-film samples upon its basis, there was no breakdown in the samples based on a high-resistivity Si ( $\rho_{\text{Si}} = 10 \Omega \text{ cm}$ ) up to the maximal value of  $(U/S) = 150 \text{ kV/m}$  used in our experiments.

Figure 2(c) shows the temperature dependence of the four-probe resistance,  $R \equiv V/I$  ( $V$  is the voltage between the inner probes, while  $I$  the current that passes between the outer ones), for a CoFe layer on a low-resistivity ( $\rho_{\text{Si}} = 5.0 \text{ m}\Omega \text{ cm}$ ) Si- $n$  substrate after discharges at different  $U/S$  values as well as for its reference, i.e., SiO<sub>2</sub>/Si- $n$ . In these experiments, we discharged  $C$  through outer probes of our four-probe device. Again, we see that, after discharges with increasing discharge voltage up to  $U/S \sim 125 \text{ kV/m}$ ,  $V/I$  of the CoFe/SiO<sub>2</sub>/Si sample approaches the value measured for the Si- $n$  substrate,  $R_{\text{Si}} \approx 0.03 \Omega$ . This can also be explained by the breakdown of SiO<sub>2</sub>. According to the measurements of the two- and four-

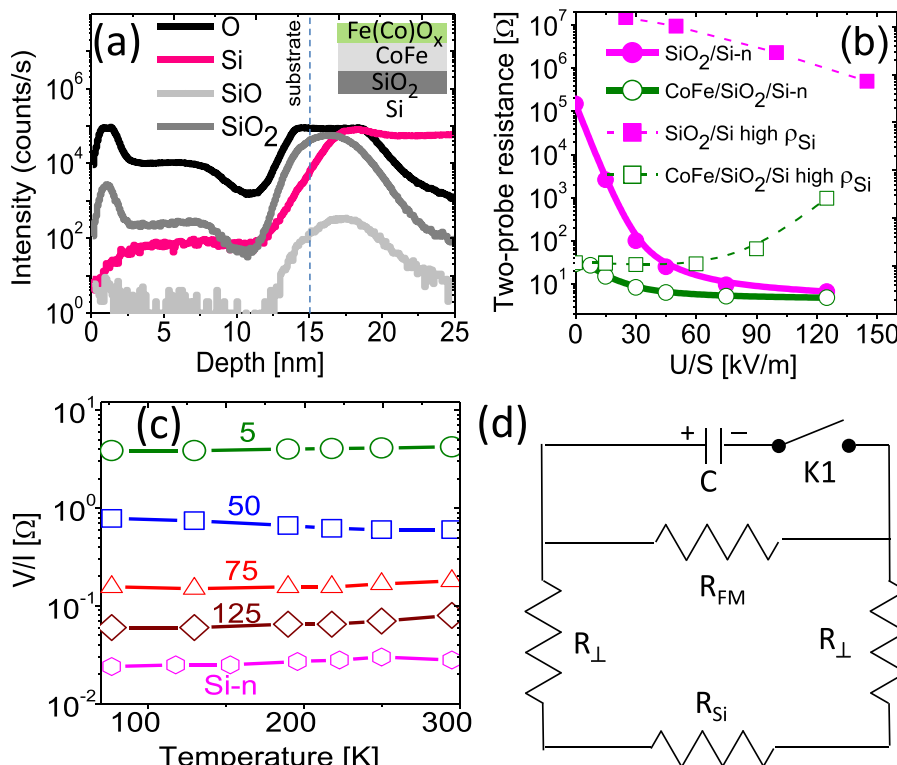


FIG. 2. (a) SIMS depth profiling of O, Si, SiO, and SiO<sub>2</sub> concentration in a 15-nm-thick CoFe/SiO<sub>2</sub>/Si- $n$  ( $\rho_{\text{Si}} = 5.0 \text{ m}\Omega \text{ cm}$ ) sample. The inset shows a sketch of the sample structure derived from the SIMS data. (b) Two-probe electric resistance in the interpad spacing versus  $U/S$  at  $C = 5.0 \mu\text{F}$  of low-resistivity Si- $n$  ( $\rho_{\text{Si}} = 5.0 \text{ m}\Omega \text{ cm}$ ) and high-resistivity Si- $p$  ( $\rho_{\text{Si}} = 10 \Omega \text{ cm}$ ) reference samples covered by SiO<sub>2</sub> and of the same samples, i.e., SiO<sub>2</sub>/Si, covered additionally by a CoFe layer. (c) Four-probe resistance,  $R \equiv V/I$ , versus temperature of the SiO<sub>2</sub>/Si- $n$  ( $\rho_{\text{Si}} = 5.0 \text{ m}\Omega \text{ cm}$ ) reference sample as well as of the CoFe/SiO<sub>2</sub>/Si- $n$  ( $\rho_{\text{Si}} = 5.0 \text{ m}\Omega \text{ cm}$ ) sample after discharges through the outer probes at different  $U/S$  values given in units of kV/m. (d) Equivalent electric scheme of the discharge circuit; see the details in the text.

probe resistances, the electric scheme of the discharge through the FM/SiO<sub>2</sub>/Si structure is shown in Fig. 2(d). After the breakdown, the transverse resistance of the SiO<sub>2</sub> layer,  $2R_{\perp}$ , becomes comparable to that of the FM layer,  $R_{\text{FM}}$ , but still remains much larger than  $R_{\text{Si}}$ . Thus,  $2R_{\perp}$  gives a major contribution to the time of a discharge through a low-resistivity Si substrate. We also note that, in the temperature range within which  $V/I$  was measured [Fig. 2(c)], its dependence on the temperature was rather weak. Such a behavior is compatible with that of thin metallic films<sup>19</sup> and of heavily doped Si ( $\rho_{\text{Si}} \sim 5.0 \text{ m}\Omega \text{ cm}$ )<sup>20</sup> studied in the same temperature regime.

In this study, we demonstrate that the breakdown of the SiO<sub>2</sub> layer in the FM/SiO<sub>2</sub>/Si structure can be used for switching of magnetization in its FM component. Initially, the magnetization was saturated in an applied magnetic field  $\mathbf{B}$  which subsequently was switched off. In the next step, we applied a bias field against the direction of the remanent magnetization  $\mathbf{M}$ —with a bias field strength  $B$  smaller than the sample coercivity,  $B_c$ . Finally, with the assistance of  $B$ , we discharged  $C$  through the sample and detected changes in the Kerr rotation, i.e., magnetization state. Figure 3 shows MOKE hysteresis cycles for three kinds of samples, (a) (15 nm)CoFe/SiO<sub>2</sub>/Si- $n$  ( $\rho_{\text{Si}} = 5.0 \text{ m}\Omega \text{ cm}$ ), (b) (20 nm)Co/SiO<sub>2</sub>/Si- $p$  ( $\rho_{\text{Si}} = 12 \text{ m}\Omega \text{ cm}$ ), and (c) (20 nm)Co/SiO<sub>2</sub>/Si- $p$  ( $\rho_{\text{Si}} = 10 \Omega \text{ cm}$ ). In all the samples studied, we observed electrically induced transitions from  $-M$  to  $+M$  and vice versa. The  $-M \leftrightarrow M$  transitions (as well as the changes to a different magnetization state such as that observed in the CoFe/SiO<sub>2</sub>/Si- $n$  sample) are shown by the arrows in Figs. 3(a)–(c)—with indications of the switching thresholds  $(U/S)_{\text{thr}}$  in units of kV/m. We mark that these  $-M \rightarrow M$  and  $M \rightarrow -M$  transitions occur at opposite directions of the discharge current. The fact of unipolarity of the switching indicates that heating of the

sample by discharge current, if happens at all, is not responsible for it. To support the latter conclusion, we calculated heating of a Si substrate and an FM layer deposited on it under capacitor discharges. The results of these calculations are presented in the [supplementary material](#). It is also striking to observe that  $(U/S)_{\text{thr}}$  strongly differs in the samples based on Si with high and low  $\rho_{\text{Si}}$  [Fig. 3(d)]. For example, we have found out that magnetization of a Co film on a low-resistivity Si ( $\rho_{\text{Si}} = 12 \text{ m}\Omega \text{ cm}$ ) substrate is switchable (shown by the double arrow) without applying  $B$  at all. In contrast, a Co film on a high-resistivity Si ( $\rho_{\text{Si}} = 10 \Omega \text{ cm}$ ) substrate exhibits the switching only if  $B$  applied is very close to  $B_c$ , while the switching thresholds for such samples are very high,  $(U/S)_{\text{thr}} > 80 \text{ kV/m}$ . This comparison highlights a key role of  $\rho_{\text{Si}}$  in the switching, which can be easily triggered in the samples with a low-resistivity Si substrate.

Finally, we confirm straightforwardly that there is a relationship between the breakdown of SiO<sub>2</sub> and the observed switching. Figure 4(a) shows a modified geometry of our experiments in which an FM (CoFe) specimen on the surface of a low-resistivity ( $\rho_{\text{Si}} = 5.0 \text{ m}\Omega \text{ cm}$ ) Si- $n$  substrate was shaped into the stripe with a width of  $\approx 1.0 \text{ mm}$  so that the electric pads could be put directly on the SiO<sub>2</sub>/Si- $n$  surface. Therefore, after the breakdown of SiO<sub>2</sub>, the discharge current flows through the Si substrate and crosses the FM specimen underneath it. In such a configuration, we have detected the switching after discharges as well. The bias fields needed for the switching and switching thresholds were close to those observed for the same sample [Fig. 3(a)] in the conventional geometry presented in Fig. 1.

Moreover, we have determined how  $\mathbf{M}$  is oriented with respect to the direction of the discharge current at which switching of  $\mathbf{M}$  does occur. As a result, according to the right-hand rule, we have concluded that, under the hypothesis that

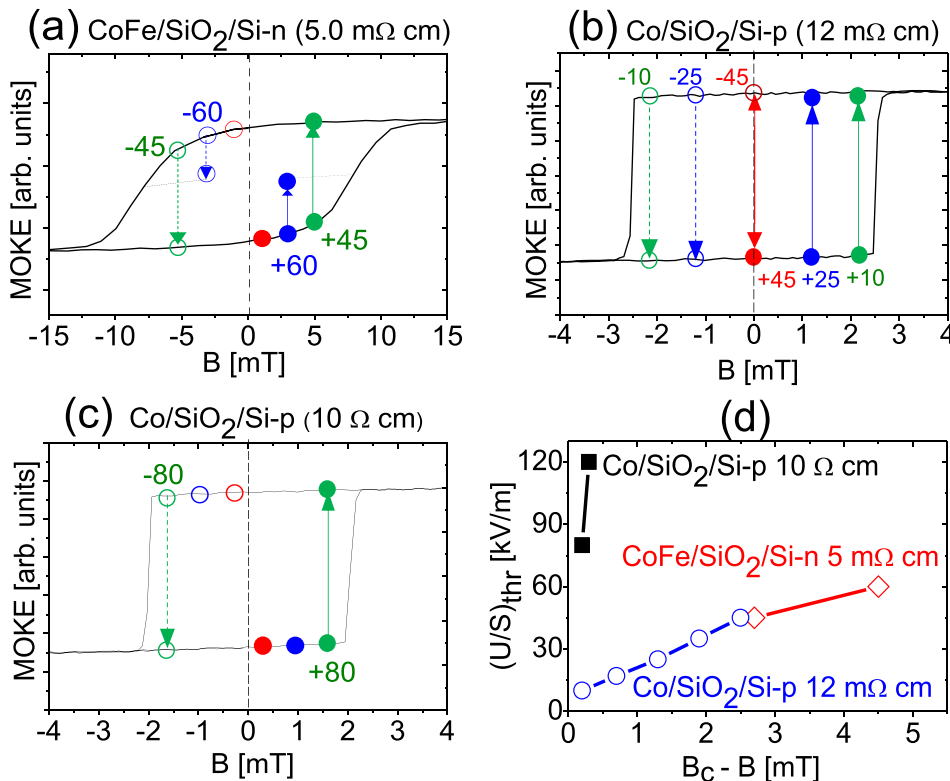


FIG. 3. (a)–(c) Hysteresis loops of 15 nm-thick CoFe and 20-nm-thick Co layers sputtered onto Si substrates of different resistivities. Electrically induced transitions in the magnetization state are indicated by the arrows. The numbers in the plots are the switching thresholds  $(U/S)_{\text{thr}}$  given in units of kV/m. (d) The switching thresholds of the samples, whose hysteresis cycles are shown in plots (a)–(c), versus  $B_c - B$ .

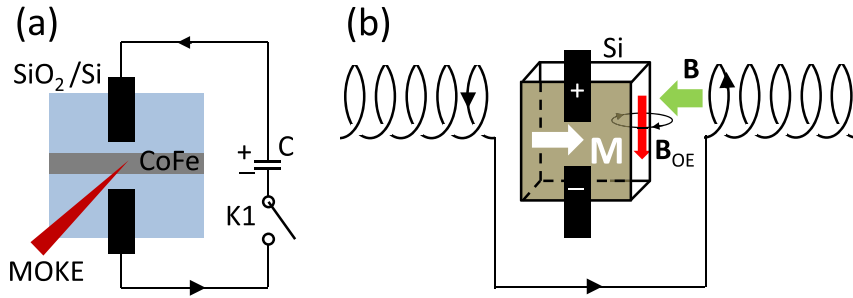


FIG. 4. (a) Modified geometry for testing electrical switching of magnetization: the FM specimen is shaped as a stripe, and electric pads lie on the SiO<sub>2</sub>/Si surface so that the discharge current should flow through the Si substrate and cross the strip-shaped CoFe specimen underneath it. (b) Identifying straightforwardly whether the discharge current flows in top or bottom of the FM layer.

$\mathbf{M}$  is switchable by  $\mathbf{B}_{\text{OE}}$ , the discharge current producing  $\mathbf{B}_{\text{OE}}$  flows through the bottom of the FM layer. This is illustrated in Fig. 4(b) where we point out the polarity of the applied voltage (the direction of the discharge current) and the direction of the electric current in the coils of an electromagnet employed for applying  $\mathbf{B}$  (and thus the direction of  $\mathbf{B}$  and  $\mathbf{M}$ ).

Within an approximation of the infinite slab of a thickness of  $d \ll S$ , the in-plane component of  $\mathbf{B}_{\text{OE}}$  produced by electric current flowing through the slab is given by (supplementary material to Ref. 10)

$$B_{\text{OE}} = \begin{cases} \frac{\mu_0 j}{2} d; & z < 0 \\ \frac{\mu_0 j}{2} (-2z + d); & 0 < z < d \\ -\frac{\mu_0 j}{2} d; & z > d, \end{cases} \quad (1)$$

where  $j$  is the current density,  $\mu_0 = 4\pi \times 10^{-7} \text{ T m A}^{-1}$  is the magnetic constant, and  $z$  is the coordinate along the normal to the slab. It follows from Eq. (1) that the average  $B_{\text{OE}}$  is equal to zero inside the slab ( $0 < z < d$ ), and so, the current flowing in the FM layer cannot affect  $\mathbf{M}$ . In FM/SiO<sub>2</sub>/Si samples with high-resistivity Si ( $\rho_{\text{Si}} \sim 10 \Omega \text{ cm}$ ), we have  $R_{\text{Si}} \gg R_{\text{FM}}$ , and so, most of the discharge current flows through the metallic FM layer. Therefore, the switching thresholds are very high in such samples [Fig. 3(d)]. In FM/SiO<sub>2</sub>/Si samples with a low-resistivity Si ( $\rho_{\text{Si}} \sim 10 \text{ m}\Omega \text{ cm}$ ) substrate, by contrast, electric current largely flows through the Si substrate [after breakdown of the SiO<sub>2</sub> layer so that  $2R_{\perp}$  would be at least  $\sim 5.0 \Omega$  (Fig. 2(b)) and thus is able to produce the outside Oersted field with its strength up to  $B_{\text{OE}} = (\mu_0/2)U/(2R_{\perp} + R_{\text{Si}})/W > 10 \text{ mT}$  that exceeds  $B_c$  in our samples. Then, the switching time can be evaluated as  $S/\mu B_{\text{OE}} \sim 50 \mu\text{s}$ , where  $\mu \sim 10 \text{ m s}^{-1} \text{ mT}^{-1}$  (Refs. 21 and 22) is the typical value of the domain-wall mobility in thin FM films. We see that the switching time evaluated is comparable to the discharge time  $2R_{\perp}C \sim 25 \mu\text{s}$  in our experiments. One should note here that the switching thresholds can be further reduced, in particular, by increasing  $C$  and thus the discharge time.<sup>10</sup>

We anticipate that the produced Oersted field can be strongly increased up to  $B_{\text{OE}} \sim 10 \text{ T}$  by achieving a deeper breakdown so that ideally  $2R_{\perp} \rightarrow 0$  in a Si wafer having  $\rho_{\text{Si}} \sim 1.0 \text{ m}\Omega \text{ cm}$  ( $R_{\text{Si}} \sim 6.0 \text{ m}\Omega$ ), which corresponds to the maximal concentration of dopants attainable currently in commercial Si wafers ( $\sim 10^{19} \text{ atoms/cm}^3$ ).<sup>23</sup> As shown in the supplementary material, electrical discharge with the parameters typical for our experiments cannot cause significant heating of Si even at extremely low  $2R_{\perp}$  and  $R_{\text{Si}}$ .

It is of great interest to apply pulsed magnetic fields— with strongly varying field strengths and pulse durations— for probing magnetization dynamics in small entities.<sup>24</sup> In particular, so far, there has been a lack of understanding of the domain-wall behavior in ferromagnetic nanowires under magnetic fields above the critical field for Walker breakdown  $\mu_0 \alpha M_s/2$  ( $\alpha \sim 0.01$  is the damping constant, and  $\mu_0 M_s$  is the saturation magnetization).<sup>21,22</sup> In view of possible applications of small magnetic entities in memory devices, it is highly desired to generate magnetic fields which would be localized at the nanoscale.<sup>25</sup> In the limit opposite to that described here, i.e.,  $d \gg S$ , the Oersted field produced by the electric current, whose density  $\mathbf{j}$  is a non-uniform function of spatial coordinates, can be numerically simulated from the equation  $\mathbf{B}_{\text{OE}} = \text{curl } \mathbf{A}$  with the vector potential satisfying the Poisson equation  $\Delta \mathbf{A} = -\mu_0 \mathbf{j}$  provided that  $\text{div } \mathbf{A} = 0$ . These studies will allow us to clarify the scalability of the  $\mathbf{B}_{\text{OE}}$  action upon a ferromagnetic entity.

We note in addition that the produced Oersted fields can be utilized in microwave magnetic devices operating in the gigahertz regime,<sup>26,27</sup> where external fields with a strength of at least a few hundred mT should be used. In such applications, the built-in magnetic field generated in FM/SiO<sub>2</sub>/Si structures could be employed instead of bulky electromagnets. We also envision the applicability of such fields in magnetic refrigeration based on the magnetocaloric effect in thin magnetic films near their ferromagnetic-paramagnetic transition.<sup>28,29</sup> A short duration of the applied field would be useful for providing the adiabaticity for the demagnetization process and thus the direct measurement of the magnetocaloric effect.<sup>30</sup> We believe that both natural and artificial SiO<sub>2</sub> layers on the Si surface can be employed in such applications.

In conclusion, we study the effect of electrical discharge on magnetization of an FM = Co, FeCo layer on a Si substrate. Our main observation is that the magnetization vector can be fully reversed even without applying a bias field. It is striking that the switching is accompanied by the dielectric breakdown of the native SiO<sub>2</sub> layer on the Si surface and that the switching threshold strongly depends on the electrical resistivity of the Si substrate. These findings enable us to conclude that the switching results from the magnetic (Oersted) field generated by the discharge current flowing through the Si substrate after the breakdown of SiO<sub>2</sub>. Utilizations of such pulsed fields in various magnetic devices fabricated on a silicon chip are feasible.

See supplementary material for evaluations of temperature elevation in a Si substrate and the thin metallic layer on it.

This work was supported by the Russian Foundation for Basic Research (RFBR) (Grant No. # 15-02-03046).

- <sup>1</sup>L. A. Kasprzak, R. B. Laibowitz, and M. Ohring, "Dependence of the SiSiO<sub>2</sub> barrier height on SiO<sub>2</sub> thickness in MOS tunnel structures," *J. Appl. Phys.* **48**, 4281–4286 (1977).
- <sup>2</sup>L. Ji, H.-Y. Hsu, X. Li, K. Huang, Y. Zhang, J. C. Lee, A. J. Bard, and E. T. Yu, "Localized dielectric breakdown and antireflection coating in metal-oxide-semiconductor photoelectrodes," *Nat. Mater.* **16**, 17–131 (2017).
- <sup>3</sup>N. Klein, "The mechanism of self-healing electrical breakdown in MOS structures," *IEEE Trans. Electron Devices* **13**, 788–805 (1966).
- <sup>4</sup>C. M. Osburn and D. W. Ormond, "Dielectric breakdown in silicon dioxide films on silicon: I. Measurement and interpretation," *J. Electrochem. Soc.* **119**, 591–597 (1972).
- <sup>5</sup>K. F. Schuegraf and C. Hu, "Reliability of thin SiO<sub>2</sub> (review article)," *Semicond. Sci. Technol.* **9**, 989–1004 (1994).
- <sup>6</sup>M. Kimura and H. Koyama, "Mechanism of time-dependent oxide breakdown in thin thermally grown SiO<sub>2</sub> films," *J. Appl. Phys.* **85**, 7671–7681 (1999).
- <sup>7</sup>X. Li, C. H. Tung, and K. L. Pey, "The nature of dielectric breakdown," *Appl. Phys. Lett.* **93**, 072903 (2008).
- <sup>8</sup>K. L. Pey, N. Raghavan, X. Wu, W. Liu, X. Li, M. Bosman, K. Shubhakar, Z. Zar Lwin, Y. Chen, H. Qin, and T. Kauerauf, "Physical analysis of breakdown in high-*j*/metal gate stacks using TEM/EELS and STM for reliability enhancement," *Microelectron. Eng.* **88**, 1365–1372 (2011).
- <sup>9</sup>W. Román Acevedo, C. Acha, M. J. Sánchez, P. Levy, and D. Rubi, "Origin of multistate resistive switching in Ti/manganite/SiO<sub>x</sub>/Si heterostructures," *Appl. Phys. Lett.* **110**, 053501 (2017).
- <sup>10</sup>N. I. Polushkin, A. C. Duarte, O. Conde, N. Bundaleski, C. Dias, J. O. Ventura, J. P. Araujo, G. N. Kakazei, P. Lupo, A. O. Adeyeye, and S. Cardoso, "Electrical switching of magnetization in a layer of  $\alpha$ -Fe with a naturally hydroxidized surface," *J. Mater. Chem. C* **4**, 7751–7755 (2016).
- <sup>11</sup>W.-G. Wang, M. Li, S. Hageman, and C. L. Chien, "Electric-field-assisted switching in magnetic tunnel junctions," *Nat. Mater.* **11**, 64–68 (2012).
- <sup>12</sup>K. Shimamura, D. Chiba, S. Ono, S. Fukami, N. Ishiwata, M. Kawaguchi, K. Kobayashi, and T. Ono, "Electrical control of Curie temperature in cobalt using an ionic liquid film," *Appl. Phys. Lett.* **100**, 122402 (2012).
- <sup>13</sup>I. M. Miron, K. Garello, G. Gaudin, P.-J. Zermatten, M. V. Costache, S. Auffret, S. Bandiera, B. Rodmacq, A. Schuhl, and P. Gambardella, "Perpendicular switching of a single ferromagnetic layer induced by in-plane current injection," *Nature* **476**, 189–194 (2011).
- <sup>14</sup>V. Uhlír, S. Pizzini, N. Rougemaille, V. Cros, E. Jiménez, L. Ranno, O. Fruchart, M. Urbánek, G. Gaudin, J. Camarero, C. Tieg, F. Sirotti, E. Wagner, and J. Vogel, "Direct observation of Oersted-field-induced magnetization dynamics in magnetic nanostripes," *Phys. Rev. B* **83**, 020406(R) (2011).
- <sup>15</sup>S. A. Gusev, D. A. Tatarskiy, A. Y. Klimov, V. V. Rogov, E. V. Skorokhodov, M. V. Sapozhnikov, B. A. Gribkov, I. M. Nefedov, and A. A. Fraerman, "Influence of the microcrystalline structure on the magnetic properties of ferromagnetic films and structures on their base," *Phys. Solid State* **55**, 481–485 (2013).
- <sup>16</sup>T. Jin, L. Hao, J. Cao, M. Liu, H. Dang, Y. Wang, D. Wu, J. Bai, and F. Wei, "Electric field control of anisotropy and magnetization switching in CoFe and CoNi thin films for magnetoelectric memory devices," *Appl. Phys. Express* **7**, 043002 (2014).
- <sup>17</sup>P. A. Yunin, Y. N. Drozdov, and M. N. Drozdov, "A new approach to express ToF-SIMS depth profiling," *Surf. Interface Anal.* **47**, 771–776 (2015).
- <sup>18</sup>P. P. Freitas and L. Berger, "Observation of s-d exchange force between domain walls and electric current in very thin Permalloy films," *J. Appl. Phys.* **57**, 1266–1269 (1985).
- <sup>19</sup>J. W. C. De Vries, "Temperature and thickness dependence of the resistivity of thin polycrystalline aluminum, cobalt, nickel, palladium, silver and gold films," *Thin Solid Films* **167**, 25–32 (1988).
- <sup>20</sup>P. W. Chapman, O. N. Tufte, J. D. Zook, and D. Long, "Electrical properties of heavily doped silicon," *J. Appl. Phys.* **34**, 3291–3295 (1963).
- <sup>21</sup>J. M. D. Coey, *Magnetism and Magnetic Materials* (Cambridge University Press, 2009).
- <sup>22</sup>G. S. D. Beach, C. Nistor, C. Knutson, M. Tsoi, and J. L. Erskine, "Dynamics of field-driven domain-wall propagation in ferromagnetic nanowires," *Nat. Mater.* **4**, 741–744 (2005).
- <sup>23</sup>See [www.svmi.com/silicon-wafers/](http://www.svmi.com/silicon-wafers/) for information about electrical resistivity of heavily doped Si wafers.
- <sup>24</sup>*Spin Dynamics in Confined Magnetic Structures II*, edited by B. Hillebrands and K. Ounadjela (Springer, Berlin, Heidelberg, 2003).
- <sup>25</sup>S. S. P. Parkin, M. Hayashi, and L. Thomas, "Magnetic domain-wall race-track memory," *Science* **320**, 190–194 (2008).
- <sup>26</sup>R. E. Camley, Z. Celinski, T. Fal, A. V. Glushchenko, A. J. Hutchison, Y. Khivintsev, B. Kuanr, I. R. Harward, V. Veerakumar, and V. V. Zagorodnii, "High-frequency signal processing using magnetic layered structures," *J. Magn. Magn. Mater.* **321**, 2048–2054 (2009).
- <sup>27</sup>J. W. Wang, S. D. Yoon, V. G. Harris, C. Vittoria, and N. X. Sun, "Integrated metal magnetic film coupled line circulators for monolithic microwave integrated circuits," *Electron. Lett.* **43**, 292–293 (2007).
- <sup>28</sup>K. A. Gschneidner, Jr., V. K. Pecharsky, and A. O. Tsokol, "Recent developments in magnetocaloric materials," *Rep. Prog. Phys.* **68**, 1479–1539 (2005).
- <sup>29</sup>T. Mukherjee, S. Sahoo, R. Skomski, D. J. Sellmyer, and C. Binek, "Magnetocaloric properties of Co/Cr superlattices," *Phys. Rev. B* **79**, 144406 (2009).
- <sup>30</sup>M. Ghorbani Zavareh, C. Salazar Mejia, A. K. Nayak, Y. Skourski, J. Wosnitzer, C. Felser, and M. Nicklas, "Direct measurements of the magnetocaloric effect in pulsed magnetic fields: The example of the Heusler alloy Ni<sub>50</sub>Mn<sub>35</sub>In<sub>15</sub>," *Appl. Phys. Lett.* **106**, 071904 (2015).